Performance of UAV-Based Digital Orthophoto Generation for Emergency Response Applications

Burak Akpınar

Yıldız Technical University, Department of Geomatics Engineering, İstanbul, Turkey

Abstract **– Unmanned Aerial Vehicles (UAVs) have been used for accurate orthophoto generation based on advanced Global Navigation Satellite System (GNSS) techniques. In recent years, the UAV systems have become an effective tool for fast monitoring of damages caused by disasters such as the earthquake hazards. The conventional orthophoto generation based on ground control points takes too much time during emergency situations. In the study, different methodologies for the processing of the acquired GNSS Positioning data for direct georeferencing of UAVs were investigated in terms of various orbit products. Evaluating the fitness for emergency response applications, the ground control points (GCPs) also used for validation of the generated orthophoto without using GCPs and based on Precise Point Positioning (PPP) approach. In this study, Ultra-Rapid, Rapid and Final PPP methods based on GNSS observations were used for direct geo-referencing. Thirteen GCPs were located at the study area for the validation of the orthophoto accuracy generated by direct geo-referencing.**

Keywords **– Unmanned Aerial Vehicles, Orthophoto, GNSS, Precise Point Positioning, Image Processing.**

DOI: 10.18421/TEM104-31
https://doi.org/10.18421/TEM104-31

Corresponding author: Burak Akpınar,
Yıldız Technical University, Department of Geomatics Engineering, İstanbul, Turkey.
Email: burakpinar@gmail.com

Received: 20 September 2021.
Revised: 24 October 2021.
Accepted: 29 October 2021.
Published: 26 November 2021.

1. Introduction

Historically, the construction of 3D models was created from analogue stereo pairs by manual orientation of stereo pairs. The advent of the Structure from Motion (SfM) algorithm brought a new paradigm in the field of photogrammetry [1]. The internal orientation parameters are calculated using ground control points (GCPs) or IMU (inertial measurement unit) + GPS (global positioning system) information [2]. Feature detection and image matching are the first steps of SfM. For this purpose, key point detection algorithms are used, such as the scale invariant feature transform (SIFT) [3]. The main steps of SIFT are scale-space extrema detection, key point localization, orientation assignment and key point descriptor [4]. After this, corresponding key points are defined by descriptors and a dense point cloud is generated [5]. The SfM digital photogrammetry technique allows precise 3D object models to be created from multiple unmanned aerial vehicle (UAV) stereo images. The 3D models generated by SfM photogrammetry are efficient for multi-scale analysis which is not comparable with traditional methods [6]. Recent developments in UAV and SfM techniques have made them a feasible option in many different applications [7]. Compared to other techniques, UAVs are more time- and cost-effective. The increase in sensor capabilities has made UAV systems very popular for civil applications [8].

This popularity has led the UAV-SfM technique to be used for different purposes to create 3D point cloud data, digital elevation models (DEMs) and digital orthophotos [9]. [10] used UAV-SfM and Light Detection and Ranging (LiDAR) data to determine and monitor topographic changes. [11] used UAV-SfM to create a DEM. The resulting DEM has been used for calculation of drift volume in quantifying snow drift on Arctic structures. [12] showed three examples of coastal zone monitoring by means of UAV-SfM technique which have a greater potential for practical applications of coastal zone monitoring. [13] reported vertical root-mean-square error (RMSE) values of 0.106 m for Test 1 with 126 GCPs and 0.097 m for Test 2 with 107

GCPs that were derived from UAV-SfM for flight altitude of 100 m. Here, the GCPs were measured by real-time kinematic (RTK) GNSS method with a better accuracy of 2 cm both horizontally and vertically. [14] calculated horizontal and vertical accuracies as 0.058m and 0.100 m respectively by UAV-SfM. They worked on a road cut-slope and the coordinates of GCPs were measured with RTK and post-processing kinematic (PPK) methods. [15] used the UAV-SfM technique for reconstruction of damaged archaeological sites. The GCPs were measured by RTK GNSS method and then all the GNSS data including UAV flight data were post-processed. They calculated horizontal, vertical, and total errors as 0.024 m, 0.026 m and 0.035 m, respectively.

As seen in the studies mentioned above, GNSS allows both RTK and PPK methods for positioning the moving UAVs and GCPs. At least two receivers are required for both RTK and PPK surveys. One receiver is located on a reference point and the other is located on a UAV. There is a communication link between these receivers during the flight in real time. If the pseudo-range data are used, the positioning accuracy of the UAV position is at the sub-meter level by differential GNSS (DGNSS) measurements. When the carrier-phase data are used in RTK applications, the position accuracy is increased to the centimeter level [16]. The limitation of the RTK method is that there are distance-dependent biases, such as orbit bias, ionosphere bias and troposphere bias. These limitations can be eliminated by establishing GNSS reference stations worldwide, named Continuously Operated Reference Systems (CORS). The Virtual Reference Station (VRS) technique is an efficient method of transmitting corrections using a data link to the users for RTK positioning [17]. The Turkish Continuously Operating Reference Stations, named CORS-TR, has been used in Turkey since 2008. The overall positioning accuracy is under 5 cm [18] with no need for a base receiver setup for UAV flights.

The Precise Point Positioning (PPP) technique [19] has developed as a powerful technique with several advantages [20] versus relative positioning methods. The one of these advantages is no base or network stations is necessary. And also, there is no need for simultaneous observations and no limit in range with the use of valid correction data [21]. The International GNSS Service (IGS) orbit/clock products are provided in various types, from the Ultra-Rapid and Rapid to the Final ephemeris [22].

Although PPP is a well-established technique, it requires a significant convergence time of 30 minutes or more to reach an accuracy of a few centimeters [23], [24]). In recent years, PPP with ambiguity resolution (PPP-AR) has been developed to improve the accuracy of the estimated coordinates and to shorten the initialization time [20], [25], [26]. PPP-AR typically involves three steps: first step is estimation of float ambiguities; second step is solving integer ambiguities; and the last step is validating the integer solution. The receiver fractional phase biases are removed by single-differencing [24]. Only by providing precise atmospheric information to PPP users, can instantaneous centimeter-level accuracy be obtained [27]. The positioning accuracy can be improved remarkably by using PPP-AR method especially in real-time processing or when the observation period is short [23] such as UAV flights. Natural Resources Canada (NRCAN) is a public provider of PPP-AR for post-processed and real-time decoupled clock (DC) products [28].

The PPP method achieved popularity after the GNSS data processing procedure became more practical by using online web-based services without the need for owning specialized software or an experienced user [26]. The GNSS data are processed by these web services based on academic softwares such as BERNESE, GIPSY/OASIS, GAMIT, etc. Canadian Spatial Reference System (CSRS), Automatic Precise Positioning Service (APPS), Magic GNSS and GNSS Analysis and Positioning Software (GAPS) are the examples of PPP online web services. The CSRS-PPP service, which is used in this study, was established by NRCAN in 2003 [29]. It is possible that single- or dual-frequency kinematic/static GNSS data can be processed free by e-mail authorization. In August 2018, the CSRS-PPP service modernized its processing engine to include PPP-AR with added single-frequency PPP positioning using code and phase observations.

[30] made an experimental analysis of GPS flight data onboard a fixed-wing small UAV with a result of 6 cm 3D positioning accuracy for a short-duration flight, such as 5 minutes, by post process kinematic PPP. They used two dual-frequency GNSS receivers and the position processes were solved by using JPL's GIPSY-OASIS and the open-source RTKLIB software. [31] made an experimental test by PPP on a fixed-wing UAV which demonstrated photogrammetric mapping at centimeter-level accuracy in planimetry and about a decimeter in height, from flights of 25 to 30 minutes duration at a flight height of 120 m. Leica Infinity software was preferred for processing the GPS PPK data. The mean differences between the PPK and GPS PPP results were about 1 to 3 cm horizontally and about 10 cm in height without GCPs. [32] achieved topographic uncertainties of ± 12 cm horizontally and ± 14 cm vertically when flying at an altitude of ~450 m above ground level of a glacier without GCPs by fixed-wing UAV.

In this study, the performance of the GNSS PPP method with the Ultra-Rapid, Rapid and Final ephemeris for UAV-based orthophoto map generation was investigated.

2. Materials and Methods

For determining the GNSS PPP performance for UAV-based digital orthophoto generation, the football stadium was selected as a test area. Thirteen GCPs were placed at the test area for the validation of the orthophoto accuracy generated by PPP direct geo-referencing. The distribution of control points is given in Figure 1.

Figure 1. The distribution of GCPs

The coordinates of the control points were determined with Network Real Time Kinematic (NRTK) positioning by using the VRS method (Figure 2) based on CORS-TR Network GNSS stations observations. Elevation angle was selected as 100 and an average of 10 observations (epoch) were used for determining the coordinates. Table 1 shows the Easting, Northing values, and the Ellipsoidal Heights (h) of the GCPs.

Figure 2. Study area and GCPs

Table 1. Coordinates of GCPs (ITRF14)

GCP	Easting (m)	Northing (m)	h (m)
1	406275.7840	4544092.7875	101.2683
2	406366.0894	4544070.5094	101.1942
3	406249.4872	4543952.7105	101.0263
4	406301.3482	4544017.4062	101.5182
5	406334.1224	4544009.0883	101.2132
6	406342.9482	4544043.9089	101.2162
7	406310.3016	4544052.5152	101.4332
8	406277.5045	4544060.9212	101.2432
9	406329.1466	4543937.6226	101.3623
10	406325.3860	4543974.1688	101.2282
11	406292.4504	4543982.6300	101.3643
12	406259.7934	4543991.1043	101.1702
13	406268.6760	4544026.0464	101.2593

In order to produce the orthophoto map, images were collected by using the DJI Phantom 4 RTK UAV at a flight height of 40 m above the ground. 80% overlap is selected for the flight plan. The trajectory of the UAV and the image positions during the flight are given in Figure 3. The test flight was done on 21st August 2019 when the weather conditions were suitable for UAV flight. The temperature was about 26º C, the sky was open, and the wind speed was suitable during the flight, which was approximately taken 10 minutes.

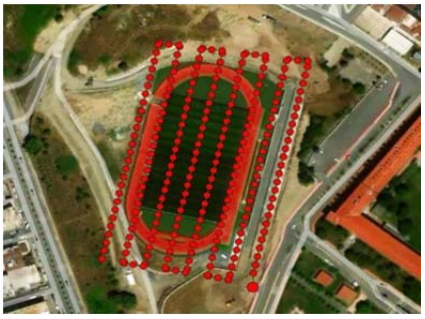

Figure 3. Flight plan and the image positions

The Phantom 4 RTK UAV Model GNSS receiver can collect data from the GPS, GLONASS and Galileo Satellite systems. Moreover, the L1&L2, B1&B2 and E1&E5a GNSS signals can be received for the GPS and GLONASS, BEIDOU and GALILEO systems, respectively. In addition, the UAV is equipped with a 20-megapixel camera with a 1" CMOS sensor and a gimbal with a pitching interval between −90° and +30° (Figure 4).

Figure 4. DJI Phantom 4 RTK flight parameters

For orthophoto generation with the Phantom 4 RTK UAV, classical RTK, NRTK as well as PPK (by using the ability to record RINEX GNSS observations) positioning methods can be used. In this study, RINEX GNSS data were recorded at a 5 Hz interval. The Phantom 4 RTK also records a Timestamp.MRK file that contains the offset of the antenna phase center to the camera CMOS center in the north-east-down coordinate system at the time the photo was taken. Also, the exposure times of the photos in UTC time are recorded in the Timestamp.MRK files. By using exposure times, it is possible to synchronize the GNSS data and photos for the PPK process.

In this study, for determining the accuracy of the GNSS PPP method in UAV digital orthophoto generation, RINEX GNSS data were processed with the Ultra-Rapid, Rapid and Final ephemeris by using the CSRS online PPP service. The PPP resulting positions were interpolated by using the offset values in the Timestamp. MRK file depending on UTC times, and the image coordinates at the exposure times resulting from the Ultra-Rapid, Rapid and Final PPP processes were obtained.

Pix4D Mapper software was used for processing the images and generating the digital orthophoto maps. At the process stage of Pix4D Mapper, image coordinates resulting from the Ultra-Rapid, Rapid and Final PPP processes were imported, and no GCP was selected for generating the digital orthophotos (Figure 5).

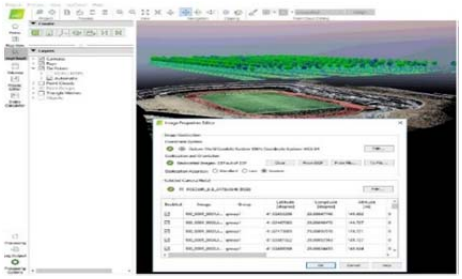

Figure 5. Pix4D Mapper process

Ultra-Rapid PPP, Rapid PPP, and Final PPP digital orthophotos were generated after the Pix4D process (Figure 6).

Figure 6. Digital orthophoto map of the study area

3. Results And Discussion

The coordinates of 13 GCPs were obtained from three generated orthophoto maps for the Ultra-Rapid, Rapid and Final PPP processes respectively. Orthophoto-based GCP co-ordinates were compared with the known GCP coordinates and the differences for the Ultra-Rapid, Rapid and Final PPP processes are given in Table 2.

Table 2. Coordinate differences of GCPs (Known – Ultra-Rapid PPP)

	Final	Rapid	Ultra-Rapid	Final	Rapid	Ultra-Rapid	Final	Rapid	Ultra-Rapid
GCPs	**Difference in Northing (cm)**			**Difference in Easting (cm)**			**Difference in Height(cm)**		
1	-0.6	4.3	2.2	-2.9	-4.4	-5.2	-1.4	-6.8	-5.9
2	0.6	6.2	4.0	-2.2	-0.2	-0.4	-0.7	-5.1	-5.1
3	1.9	-0.4	-2.2	-2.7	-5.7	-6.0	-0.5	-5.1	-4.7
4	0.6	2.3	0.1	-1.6	-3.2	-2.8	-0.3	-9.4	-9.1
5	0.8	1.7	0.5	-2.2	-0.7	-1.4	1.2	-8.9	-8.0
6	0.1	3.9	1.6	-2.4	-0.4	-1.3	1.5	-8.3	-8.1
7	-0.6	3.8	2.0	-2.8	-2.6	-3.2	1.2	-7.7	-6.9
8	2.5	5.0	3.3	-2.6	-4.4	-5.1	-2.8	-9.3	-8.9
9	0.5	-1.6	-2.4	-2.9	-2.5	-2.9	-0.9	-3.7	-3.3
10	2.0	0.9	0.0	-2.7	-1.4	-1.2	3.7	-6.5	-6.4
11	-0.5	-0.7	-2.6	-2.7	-4.0	-4.3	0.3	-8.5	-8.0
12	0.9	1.4	0.5	-2.9	-5.0	-5.7	-0.1	-9.9	-8.9
13	2.6	2.2	1.7	-3.2	-5.5	-6.4	-1.2	-10.1	-9.1

Table 3. Summary of coordinate differences

PPP Method	**Minimum (cm)**			**Maximum (cm)**			**Mean (cm)**			**Standard Deviation (cm)**		
Ultra-Rapid	-2.6	-6.4	-9.08	4.0	-0.4	-3.3	0.7	-3.5	-7.1	2.1	2.1	1.9
Rapid	-1.6	-5.7	-10.07	6.2	-0.2	-3.7	2.2	-3.1	-7.6	2.4	1.9	2.1
Final	-0.6	-3.2	-2.78	2.6	-1.6	3.7	0.8	-2.6	0.0	1.1	0.4	1.6
Coordinates Diff.	**Northing**	**Easting**	**Height**	**Northing**	**Easting**	**Height**	**Northing**	**Easting**	**Height**	**Northing**	**Easting**	**Height**

According to the results based on three different orbit products demonstrate that similar results are obtained from the three different PPP processing methods. The coordinate differences in northing, easting, and height for the three PPP methods are shown in Figure 7, Figure 8 and Figure 9 respectively. The minimum, maximum and mean values and standard deviations of differences are given in Table 3 as a summary of the results.

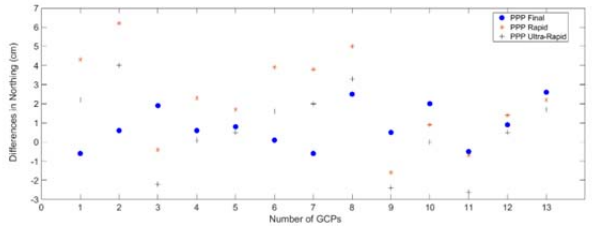

Figure 7. Coordinate differences in northing for PPP methods

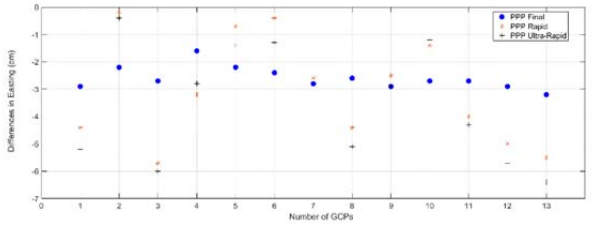

Figure 8. Coordinate differences in easting for PPP methods

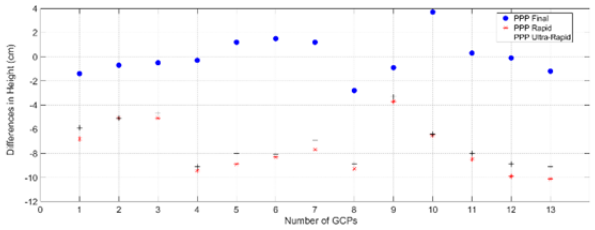

Figure 9. Coordinate differences in height for PPP methods

In the Table 3, the overall accuracy is represented for two different orbit products (ultra-rapid and rapid) generated by International GNSS Service for real time or near real time positioning. The final orbit product also evaluated for the upper limit of accuracy that can be used for post processing scenarios.

4. Conclusion

Using a direct georeferencing approach in photogrammetry is a challenging factor of validating the geometric accuracy of generated orthophoto without GCP checkpoints. In this study, 13 GCP checkpoints were used to investigate the orthophoto generation accuracy by direct georeferencing based on PPP approach.

As can be seen in Table 2, the Ultra-Rapid, Rapid and Final PPP methods produce 2.1 cm for horizontal while 4.9 cm for vertical accuracy. Furthermore, the standard deviations demonstrate that the confidence of the obtained accuracy is sufficient for urgent mapping applications. As a conclusion, the orthophoto generation without using GCPs and based on PPP method provide 3.5 cm accuracy for 3 dimensional spaces when the whole coordinate components evaluated together. On the other hand, the approach of PPP needs a convergence time due to the restriction of ambiguity resolution techniques especially for real time kinematic applications. If the study area is covered by Active GNSS Network, the NRTK techniques (VRS: Virtual Reference Stations, FKP: Flachen Korrectur Parameter and MAC: Master Auxiliary Concept) can be used instead of absolute positioning techniques to avoid time consuming convergence time. However, the PPP technique gives an opportunity for providing position information, which can be used anywhere in the world and is accurate for emergency situations, even with fast orbit products. Ultra-Rapid PPP method can be used to determine the image exposure time coordinates instead of waiting for the final ephemeris information.

In terms of the image processing stage of UAV orthophoto production, choosing GCPs causes a significant time loss. In addition, if GCPs were used, they should be measured and processed by geodetic techniques or GNSS methods before UAV flights. De-pending on the number of GCPs which are to be established according to the characteristics of the flight area, the geodetic measurements to determine the GCP coordinates cause significant time loss and indirect cost increase.

Consequently, many studies in the literature suggest using a small number of GCPs as a validation input in order to avoid and correct the random GNSS positioning errors [33]. However, the results demonstrate that without using the GPCs, the accuracy of the PPP technique for the orthophoto generation provide sufficient results especially for maps needed in emergency situations such as in earthquake, fire or search and rescue operations.

The usability of the method examined in this study in wider areas can be determined by additional studies. For example, testing the PPP GNSS direct geo-referencing method in areas with different topographic structures will contribute to determining the usability of the method in different areas. It has been determined with this study that in areas where the topography does not change much, sufficient results can be obtained with the PPP GNSS direct geo-referencing method.

Acknowledgements

The authors wish to acknowledge the Canadian Geodetic Survey of Natural Resources Canada for processing data using the CSRS PPP online web service.

References

[1]. Feurer, D., & Vinatier, F. (2018). Joining multi-epoch archival aerial images in a single SfM block allows 3-D change detection with almost exclusively image information. *ISPRS journal of photogrammetry and remote sensing*, *146*, 495-506. https://doi.org/10.1016/j.isprsjprs.2018.10.016

[2]. Westoby, M. J., Brasington, J., Glasser, N. F., Hambrey, M. J., & Reynolds, J. M. (2012). 'Structure-from-Motion'photogrammetry: A low-cost, effective tool for geoscience applications. *Geomorphology*, *179*, 300-314. http://dx.doi.org/10.1016/j.geomorph.2012.08.021

[3]. Lowe, D. G. (2004). Distinctive image features from scale-invariant keypoints. *International journal of computer vision*, *60*(2), 91-110.

[4]. Hughes, R. A. (2011). Geoscience data and derived spatial information: Societal impacts and benefits, and relevance to geological surveys and agencies. *Geological Society of America Special Papers*, *482*, 35-40. https://doi.org/10.1130/2011.2482(04)

[5]. Murtiyoso, A., & Grussenmeyer, P. (2017). Documentation of heritage buildings using close-range UAV images: dense matching issues, comparison and case studies. *The Photogrammetric Record*, *32*(159), 206-229. https://doi.org/10.1111/phor.12197

[6]. Dering, G. M., Micklethwaite, S., Thiele, S. T., Vollgger, S. A., & Cruden, A. R. (2019). Review of drones, photogrammetry and emerging sensor technology for the study of dykes: Best practises and future potential. *Journal of Volcanology and Geothermal Research*, *373*, 148-166. https://doi.org/10.1016/j.jvolgeores.2019.01.018

[7]. O'Driscoll, J. (2018). Landscape applications of photogrammetry using unmanned aerial vehicles. *Journal of Archaeological Science: Reports*, *22*, 32-44. https://doi.org/10.1016/j.jasrep.2018.09.010

[8]. Agueera-Vega, F., Carvajal-Ramirez, F., Martinez-Carricondo, P., López, J. S. H., Mesas-Carrascosa, F. J., Garcia-Ferrer, A., & Pérez-Porras, F. J. (2018). Reconstruction of extreme topography from UAV structure from motion photogrammetry. *Measurement*, *121*, 127-138. https://doi.org/10.1016/j.measurement.2018.02.062

[9]. Hastaoğlu, K. Ö., Gül, Y., Poyraz, F., & Kara, B. C. (2019). Monitoring 3D areal displacements by a new methodology and software using UAV photogrammetry. *International Journal of Applied Earth Observation and Geoinformation*, *83*, 101916. https://doi.org/10.1016/j.jag.2019.101916

[10]. Izumida, A., Uchiyama, S., & Sugai, T. (2017). Application of UAV-SfM photogrammetry and aerial lidar to a disastrous flood: repeated topographic measurement of a newly formed crevasse splay of the Kinu River, central Japan. *Natural Hazards and Earth System Sciences*, *17*(9), 1505-1519.

[11]. Hawley, R. L., & Millstein, J. D. (2019). Quantifying snow drift on Arctic structures: A case study at Summit, Greenland, using UAV-based structure-from-motion photogrammetry. *Cold Regions Science and Technology*, *157*, 163-170. https://doi.org/10.1016/j.coldregions.2018.10.007

[12]. Castellanos-Galindo, G. A., Casella, E., Mejía-Rentería, J. C., & Rovere, A. (2019). Habitat mapping of remote coasts: Evaluating the usefulness of lightweight unmanned aerial vehicles for conservation and monitoring. *Biological Conservation*, *239*, 108282. https://doi.org/10.1016/j.biocon.2019.108282

[13]. Hugenholtz, C. H., Walker, J., Brown, O., & Myshak, S. (2015). Earthwork volumetrics with an unmanned aerial vehicle and softcopy photogrammetry. *Journal of Surveying Engineering*, *141*(1), 06014003. https://doi.org/10.1061/(ASCE)SU.1943-5428.0000138

[14]. Carvajal-Ramírez, F., Agüera-Vega, F., & Martínez-Carricondo, P. J. (2016). Effects of image orientation and ground control points distribution on unmanned aerial vehicle photogrammetry projects on a road cut slope. *Journal of Applied Remote Sensing*, *10*(3), 034004.

[15]. Carvajal-Ramírez, F., Navarro-Ortega, A. D., Agüera-Vega, F., Martínez-Carricondo, P., & Mancini, F. (2019). Virtual reconstruction of damaged archaeological sites based on Unmanned Aerial Vehicle Photogrammetry and 3D modelling. Study case of a southeastern Iberia production area in the Bronze Age. *Measurement*, *136*, 225-236.

[16]. Langley, R. B. (1998). Rtk gps. *Gps World*, *9*(9), 70-76.

[17]. Rizos, C., & Han, S. (2003). Reference station network based RTK systems-concepts and progress. *Wuhan University Journal of Natural Sciences*, *8*(2), 566-574.

[18]. Eren, K., Uzel, T., Gulal, E., Yildirim, O., & Cingoz, A. (2009). Results from a comprehensive Global Navigation Satellite System test in the CORS-TR network: Case study. *Journal of Surveying Engineering*, *135*(1), 10-18. https://doi.org/10.1061/(ASCE)0733-9453(2009)135:1(10)

[19]. Zumberge, J. F., Heflin, M. B., Jefferson, D. C., Watkins, M. M., & Webb, F. H. (1997). Precise point positioning for the efficient and robust analysis of GPS data from large networks. *Journal of geophysical research: solid earth*, *102*(B3), 5005-5017.

[20]. Zou, X., Tang, W., Shi, C., & Liu, J. (2015). Instantaneous ambiguity resolution for URTK and its seamless transition with PPP-AR. GPS solutions, 19(4), 559-567. https://dx.doi.org/10.1007/s10291-014-0411-7

[21]. Huber, K., Abart, C., Heuberger, F., Karabatic, A., Weber, R., & Berglez, P. (2010). PPP: Precise Point Positioning–Constraints and Opportunities. In *XXIV FIG International Congress 2010* (pp. 1-17).

[22]. Kouba, J. (2009). A guide to using International GNSS Service (IGS) products. Retrieved from: http://acc.igs.org/UsingIGSProductsVer21.pdf [accessed: 10 June 2021].

[23]. Geng, J., Chen, X., Pan, Y., Mao, S., Li, C., Zhou, J., & Zhang, K. (2019). PRIDE PPP-AR: an open-source software for GPS PPP ambiguity resolution. *GPS Solutions*, *23*(4), 1-10. https://doi.org/10.1007/s10291-019-0888-1

[24]. Deo, M., & El-Mowafy, A. (2018). Triple-frequency GNSS models for PPP with float ambiguity estimation: performance comparison using GPS. *Survey review*, *50*(360), 249-261. https://doi.org/10.1080/00396265.2016.1263179

[25]. Li, X., Li, X., Yuan, Y., Zhang, K., Zhang, X., & Wickert, J. (2018). Multi-GNSS phase delay estimation and PPP ambiguity resolution: GPS, BDS, GLONASS, Galileo. *Journal of geodesy*, *92*(6), 579-608. https://doi.org/10.1007/s00190-017-1081-3

[26]. Bezcioglu, M., Yigit, C. O., & El-Mowafy, A. (2019). Kinematic PPP-AR in Antarctic. *Sea Technology*, *60*(2), 20-23.

[27]. Laurichesse, D., & Banville, S. (2018). Innovation: Instantaneous centimeter-level multi-frequency precise point positioning. *GPS World J*, *29*(4).

[28]. Seepersad, G., & Bisnath, S. (2017). An assessment of the interoperability of PPP-AR network products. *The journal of global positioning Systems*, *15*(1), 1-12. https://dx.doi.org/10.1186/s41445-017-0009-9

[29]. Alkan, R. M., Saka, M. H., Ozulu, İ. M., & İlçi, V. (2017). Kinematic precise point positioning using GPS and GLONASS measurements in marine environments. *Measurement*, *109*, 36-43. https://doi.org/10.1016/j.measurement.2017.05.054

[30]. Gross, J. N., Watson, R. M., D'Urso, S., & Gu, Y. (2016). Flight-Test Evaluation of Kinematic Precise Point Positioning of Small UAVs. *International Journal of Aerospace Engineering*, *2016*, 1-11. http://dx.doi.org/10.1155/2016/1259893

[31]. Grayson, B., Penna, N. T., Mills, J. P., & Grant, D. S. (2018). GPS precise point positioning for UAV photogrammetry. *The photogrammetric record*, *33*(164), 427-447. https://dx.doi.org/10.1111/phor.12259

[32]. Chudley, T. R., Christoffersen, P., Doyle, S. H., Abellan, A., & Snooke, N. (2019). High-accuracy UAV photogrammetry of ice sheet dynamics with no ground control. *The Cryosphere*, *13*(3), 955-968. https://doi.org/10.5194/tc-13-955-2019

[33]. Harwin, S., Lucieer, A., & Osborn, J. (2015). The impact of the calibration method on the accuracy of point clouds derived using unmanned aerial vehicle multi-view stereopsis. Remote Sensing, 7(9), 11933-11953. doi: 10.3390/rs70911933.